Glassy Carbon μECoG Electrode Array for In-vivo Sensing and Stimulation

Tyler Maxfield

A thesis
submitted in partial fulfillment of the
requirements for the degree of

Master of Science in Bioengineering

University of Washington

2015

Committee:

Eberhard Fetz, Chair

James B Bassingthwaighte

Steve I Perlmutter

Program Authorized to Offer Degree:
Bioengineering

University of Washington

Abstract

Glassy Carbon μECoG Electrode Array for In-vivo Sensing and Stimulation

Tyler Maxfield

Chair of the Supervisory Committee:
Professor Eberhard Fetz
Physiology and Biophysics

Current neural-prosthetic devices fail to provide high-quality signals with good resolution for long periods of time. This is due to changes in the device-tissue interface, mostly in the form of device degradation and macrophage/microglia encapsulation. A novel material for neural interfaces, glassy carbon (GC) provides tunable stiffness and impedance, reducing mechanical strain on brain tissue and offering optimized charge injection capabilities. GC is often used in electrochemical reactions due to its high stability and resistance to corrosion. Holes were also integrated into the design to allow astrocytes to form around the device, securing it in place for stable recording locations. We present results from in-vivo testing of a fully customized neural device made of GC μECoG electrodes and metal traces, supported on a flexible, polyimide substrate. The devices were integrated into a custom PCB using a low profile connector. They were then implanted subdurally into the brains of rats. During implant, complex impedance was measured multiple times weekly as an indicator of changes in the tissue-device interface. Stimulation effectiveness was determined by testing for evoked potentials. Animals were implanted with electrodes for 5-6 weeks, after which the animals were sacrificed for histological analysis. Our results led us toward several design modifications before we had a fully functioning device. We also found that the holes performed as hypothesized and allowed for astrocytes to anchor the device.

TABLE OF CONTENTS

LIST OF FIGURES

GLOSSARY

COMPLEX IMPEDANCE: A measurement of an electrical circuit that describes the frequency dependance of the real and imaginary components of energy loss.

BUMP PADS: The part of the μECoG array that electrically interfaces with the ZIF connector. Bump pads are rectangular patches of exposed metal.

μECoG: An electrical potential recording interface that is placed directly on the cortex of the brain.

EVOKED POTENTIAL: A recorded neural response at one electrode site that is caused by a stimulation event at another electrode site.

GLASSY CARBON: A conductive carbon structure made from the pyrolysis of SU-8 photoresist.

OUTPUT LIMIT: The maximum voltage that a stimulator can generate.

PCB: Printed Circuit Board. Electrically connects and mechanically supports multiple electrical components. Constructed out of conductive copper traces laminated on to a non-conductive material.

ZIF: Zero Insertion Force connector. A type of connector that accepts a thin film μECoG device to electrically interface with a PCB.

ACKNOWLEDGMENTS

The author wishes to express sincere appreciation to Eberhard Fetz and Steve Perlmutter for their support and advice throughout the research process. To Robert Robinson, without whom this project would have been orders of magnitude more difficult and time consuming. To Brian Mogen and Stephanie Seeman for their expertise and patience. To the University of Washington, where he has had the opportunity to work with many talented individuals and where countless opportunities were presented. Last but not least, to Maria Vomero and Ian Dryg, whose collaboration on this project was beyond valuation. Thank you all.

Chapter 1

INTRODUCTION

In areas of research and medicine, neural implants have shown incredible impact and are expanding in their scope of use. Diseases such as essential tremor[15], epilepsy[10][14] and Parkinson's[15] can now be managed by deep brain stimulators, patients are now being implanted with electrode arrays over the retina to treat blindness[6][8], and research suggests that neural implants can be used to treat stroke and spinal cord injuries[20][13][9]. The clinical success of DBS has led researchers to investigate their applicability to a myriad of neurological diseases, such as depression and schizophrenia[16]. Retinal implants have shown great success in treating retinitis pigmentosa[6], leading to their recent trial use to treat macular degeneration[8]. To do these things requires repeated neural stimulation and/or recording. However, implanted neural electrodes cause a tissue response which surrounds the implant over time, eventually preventing neural signals from reaching the electrodes and causing them to fail after months to years.

1.1 Tissue Response to Implantation

Neural electrode failure is related to a dynamic two-part tissue response by the host - an initial response due to the damage done by electrode insertion, and a secondary response due to the chronic presence of the electrode in the neural tissue[17]. Electrodes that were inserted and immediately removed yielded no scar after 4 weeks, suggesting that neural tissue is able to recover from such acute damage[2]. It is thought that minimizing acute damage helps to minimize the chronic response. If the electrode remains within neural tissue over an extended period of time, then the initial acute injury evolves into an irreversible, chronic tissue response[2][21]. During this tissue response, macrophages, microglia and astrocytes are

observed to become activated: they withdraw their processes, migrate towards the implanted electrodes, and attempt to engulf the electrodes. Because the electrodes are so large, the cells cannot engulf them, so they clump together to form a multi-nucleated mass, walling off the electrode from the rest of the brain.

As a result of the tissue response, impedance and phase delay of the electrodes increases. This is partly due to deposition of extracellular matrix by the astrocytes and microglia, as well as the cell bodies themselves[24]. As impedance increases, the signal of interest decreases in amplitude, while noise increases. This cellular deposition and growth also causes the cells of interest to be farther away from the surface of the electrode. These factors cause a decrease in the signal-to-noise ratio (SNR). Eventually most of the neuronal signals are lost over the course of months to years[12][22][23]. In order to be clinically successful, these neural interfaces should be functional for many years before needing to be replaced.

Many attempts have been made to reduce the tissue response surrounding implantable neural electrodes. Smaller electrode size[19], less stiff materials[5][7], sharper electrode tips and faster insertion speeds[3] all seem to reduce damage during insertion and cause a less severe chronic tissue response. These techniques focus mostly on penetrating electrodes and researchers are only just beginning to consider how to design surface electrodes such that they cause less of a tissue response[18].

Currently, the best way to evaluate the tissue response at a cellular level is to use post-mortem histology. There are techniques to monitor the tissue response in vivo, yet they rely on indirect measurements. There are no techniques presently available to directly monitor the tissue response in vivo, as modern imaging modalities do not provide sufficient resolution for a cellular measurement in sub-surface brain structures.

1.1.1 Complex Impedance

For this study, complex impedance (CI) was the chosen method to characterize changes in electrical impedance of these implants because CI provides a good, indirect measurement of changes in the device-tissue interface[24][18]. In general, the real component gives infor-

mation about the resistance of the implanted device and nearby tissue while the imaginary component gives capacitance information about the device-tissue interface and surrounding tissue. When measuring CI with a potentiostat, the voltage between two points is controlled while the resulting current is measured. The voltage is cycled at different frequencies and measurements of the real and imaginary components of impedance (magnitude and phase) are collected. These recordings provide information about the capacitive and resistive elements of the device-tissue circuit. The equation that describes complex impedance is: $Z = R + jX$, where the magnitude $|Z|$ is the ratio of voltage amplitude (input, figure 1.1) over the current amplitude (output), R is the real resistance, j is the imaginary unit and X is the imaginary resistance (called reactance).

The imaginary component of CI is related to the capacitance of the tissue-device circuit. Cellular membranes act as semi-capacitive elements because the lipid bilayers are barriers against charge transfer, maintaining a voltage difference across the membrane that takes time to equalize. This increased charge transfer time causes a phase delay between the measured current and the applied voltage (figure 1.1). It also gives information about the rate of charge transfer between the electrode and ionic solution. In general, an increased phase indicates an increased cellular response[24].

Of particular interest is the magnitude of impedance at 1kHz. This value is biologically relevant because the inverse time it takes a neuron to depolarize and repolarize (about 2ms) is equivalent to 500Hz. The Nyquist rate for recording such a signal is 1kHz. The magnitude of impedance at 1kHz has thus become the standard value at which to compare neural electrodes. This information also gives insight into the health of the implanted electrodes. If the magnitude of impedance were to suddenly increase, it would indicate a break in the metal trace leading up to the electrode or a fissure in the electrode itself. If the magnitude of impedance were to suddenly decrease, it would indicate deinsulation somewhere along the μECoG array.

High impedance of neural electrodes are problematic for two reasons. Foremost is that we are unable to stimulate at the current amplitudes necessary to evoke neural activity. A

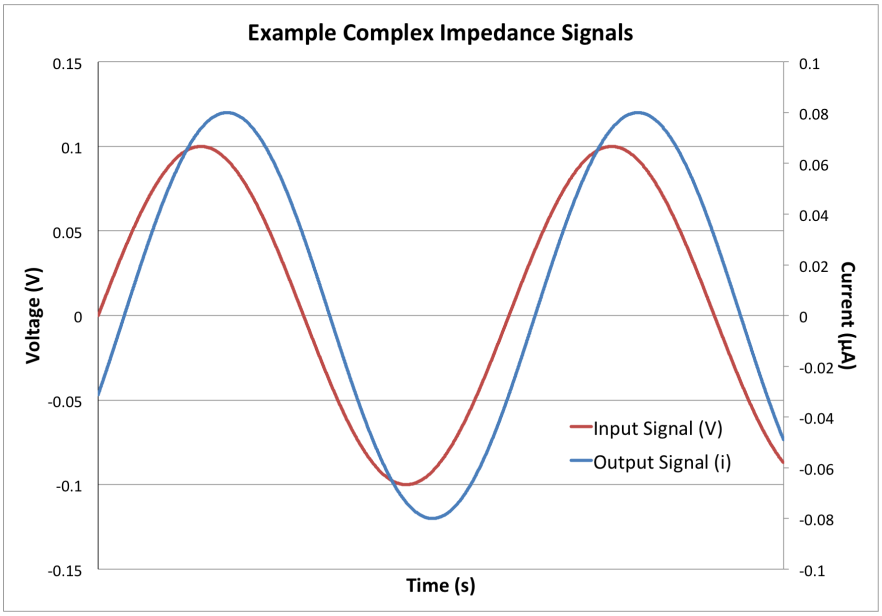

Figure 1.1: Example signal that is used to calculate magnitude and phase values during complex impedance measurement.

simple calculation of Ohm's law shows that in order to get a current (i) of $100\mu A$ out of a device that has a resistance (R) of $1\text{M}\Omega$ we would need to have a stimulator capable of $100V$. This is impractical because the high voltage version of the Neurochip 2.0 is only capable of 50V and the standard design is capable of 10V. Furthermore, the high impedance presents a problem when trying to measure small voltages (under 1mV) because the electrical current must travel along a high impedance trace, losing energy along the way. In general, high impedance electrodes are used for very local measurements, such as intracellular recordings, whereas low impedance electrodes are used for broad field measurements. ECoG is a broad field measurement.

1.2 Tissue Response to Stimulation

During electrical stimulation, the charge carrier must be converted between electron flow, in the metallic components, to ionic flow, in the tissue. The Warburg constant describes the

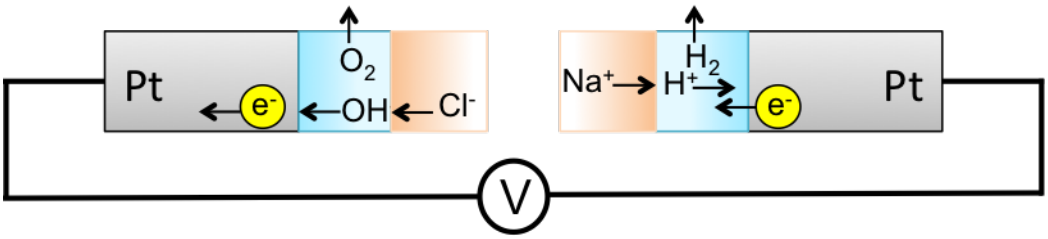

Figure 1.2: Electrical stimulation using a platinum electrode in saline solution.

rate at which this interchange can take place, limited by the diffusion of ions away from the electrode surface. When stimulating below the water window, the voltage bounds outside which water is split into H^+ and OH^-, typically -0.6V to +0.8V[1], the charge carriers are ions. In saline, as the electron exits the negative electrode it reacts with electrostatically-attracted Na^+, causing the ion to be absorbed. At the opposing interface, Cl^- donates an electron, completing the circuit. These reactions cause the net current flow in electrolyte solution. It is this ionic charge balancing that causes neural depolarization due to electrical stimulus.

When stimulating outside the water window an additional reaction takes place. As the electron exits the negative electrode it reacts with electrostatically-attracted hydrogen ions according to the following equation: $4H^+ + 4e^- -> 2H_2$. At the opposing interface, the following reaction takes place: $4OH^- -> 2H_2O+O_2+4e^-$ resulting in a balance of charge[11] (figure 1.2). The Perlmutter and Fetz labs often perform stimulation outside the water window, making it necessary to have an electrode that can withstand repeated exposure to strong reductive and oxidative reactions.

1.2.1 Stimulation of Monkey Motor Cortex

In a previous study, I found that chronic stimulation of macaque motor cortex does have an effect on the long-term tissue response at the tissue-implant interface. For this study,

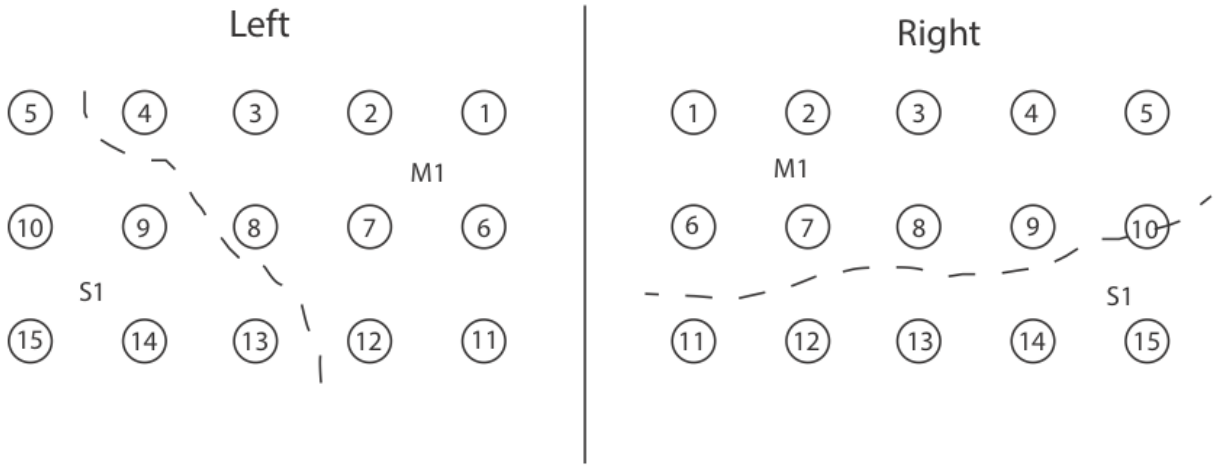

Figure 1.3: Diagram depicting the relative electrode placement in monkey cortex. Each circle represents the location of both an epidural and intracortical electrode.

stimulation occurred in the left hemisphere only on electrodes 3, 7 and 11. The right hemisphere went unstimulated (figure 1.3). I found the linear slope relation between the negative imaginary and real components of the CI measurements to calculate, using n-dimensional ANOVA, the comparison between population variance and the variance attributed to the factors: electrode depth (epidural or intracortical), stimulation (yes or no), and time (beginning, middle, and end). It was determined that stimulation ($p = 0.0214$) was one of the factors that caused the variability of CI measurements seen in figure 1.4. This figure shows CI data collected from epidural and intracortical microwire electrodes over three months of implantation. Each color represents CI traces collected from a single day, ranging from blue to red. Looking at the variance between subfigures A and B and subfigures C and D, one can see that over the course of the experiments the spread of of the imaginary-real slopes was much greater in the left hemisphere compared the right. Cellular changes in the device-tissue interface would cause these slopes to change, suggesting that there is a tissue response to stimulation.

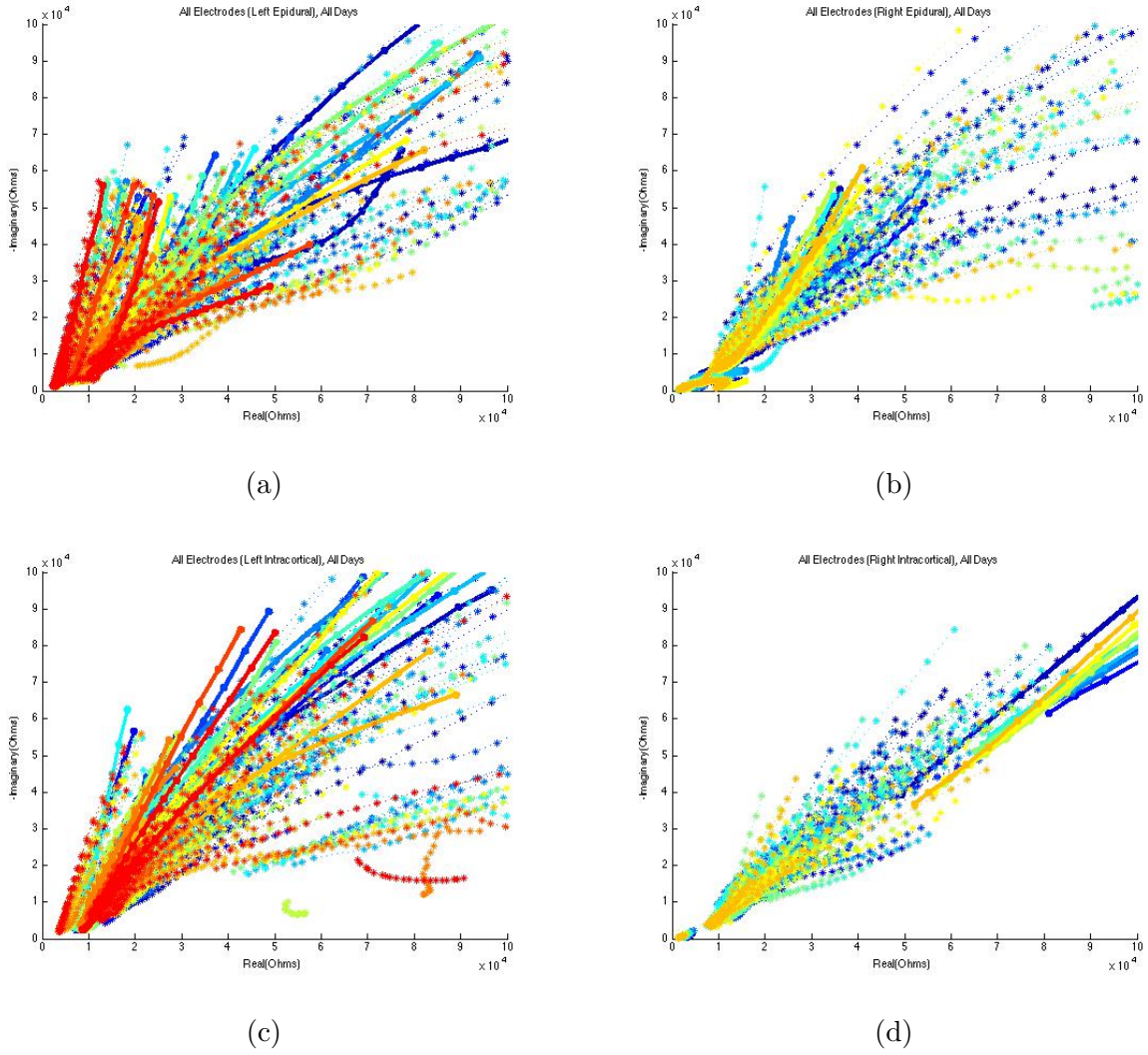

(a) (b)

(c) (d)

Figure 1.4: Left epidural (a), right epidural (b), left intracortical (c) and right intracortical (d) electrodes complex impedance results. All electrodes for a given day are plotted in the same color. Color varies between days from blue to red.

1.3 Glassy Carbon

Neural electrodes must be made of materials that are biocompatible. Early fabrication techniques included filling heat-pulled glass tubes with an electrolyte solution[11]. A more flexible alternative is to manually assemble an array of metal microwires constructed from biocompatible metals such as stainless steel or platinum and insulated with biocompatible materials such as polyimide or polytetrafluoroethylene (commercially known as Teflon)[11]. Microelectro-mechanical systems (MEMS) technology is a modern fabrication technique that has allowed for microfabrication of electrode arrays to a high degree of uniformity while allowing for increased electrode density.

Using MEMS also allows for the integration of novel materials in electrode fabrication. GC is an promising material for a neural interfaces because the mechanical stiffness, hardness, impedance and charge injection are able to be controlled[7] (figure 1.5) by changing the pyrolysis temperature and time. GC has characteristics that are more similar to neural tissue than conventional electrodes[7] (figure 1.6). For example, the mechanical stiffness (E) and hardness (H) are an order of magnitude smaller than the Michigan and Utah arrays, which are widely used in neural research. These lower hardness and stiffness values allow for better mechanical matching to the tissue, potentially resulting in reduced tissue response to implantation. In order to make the best use of GC properties, polyimide was used as the array substrate because it is even softer than GC.

ECoG is a minimally invasive neural implant that offers high density signals with physiologically meaningful information. ECoG uses electrodes that are placed directly on the surface of the brain, thereby avoiding tissue trauma caused by intracortical electrodes. These surface electrodes measure local potentials as an indicator of the summed ionic current flow within the region. For this study we used two types of devices, GC and platinum electrodes. The platinum electrodes had contacts on the same side as the bump pads (which are rectangular patches of exposed metal that interface with a connector) and the GC electrodes had contacts on the opposite side of the bump pads. This allowed us to make inferences

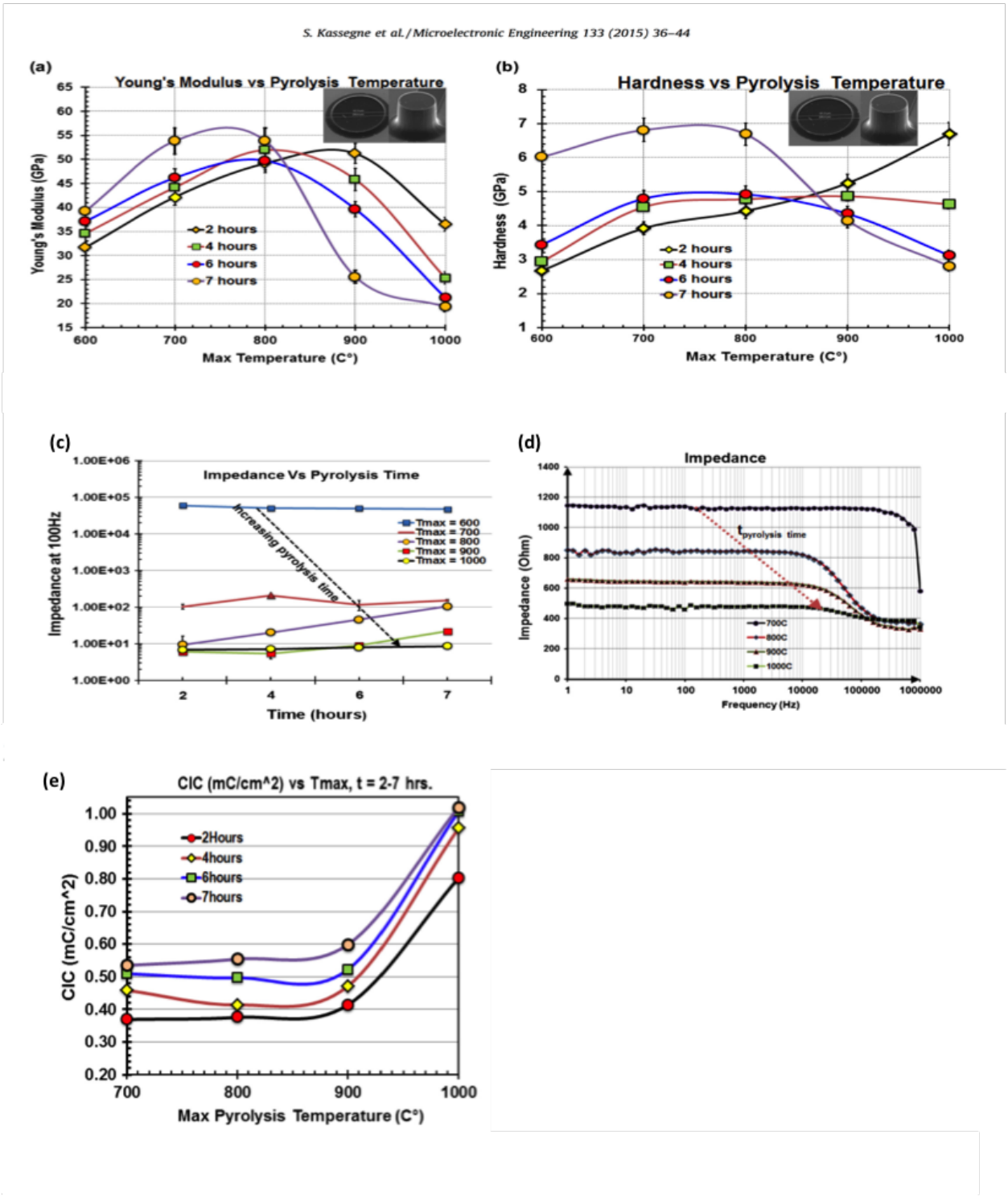

Figure 1.5: The pyrolysis temperature and time dependance of glassy carbon's: A) Young's modulus, B) hardness, C/D) impedance, and E) charge injection. [7]

Table 3
Summary of electrical and mechanical properties of tissues.

Tissue	Impedance at 1 kHz (Ω)	*E*	*H*
Cortex	For intercortical recording, 50 Ω–1 MΩ [35]	0.5–1 kPa [43]	NA
Spinal	Impedance for spinal cord signal recording, 50–150 kΩ	1.5 MPa with Pia mater 0.1 MPa, no Pia mater [44]	NA
Utah microarray	100–300 kΩ [45]	160–170 GPa	13 GPa
Michigan microarray	~100–400 kΩ [46]	160–170 GPa	13 GPa
Polyimide electrodes	6 kΩ	3–4 GPa (only substrate)	0.1 GPa
Parylene C	6 kΩ	2.8–3 GPa (only substrate)	0.26 GPa
Current study	10 Ω–100 kΩ (at 1 kHz)	20 GPa (electrodes)	3–6 GPa

Figure 1.6: A comparison of impedance, elasticity, and hardness for several different tissue types and electrode materials. Glassy carbon is listed as "current study" on the table and shows significantly lower values for each category, making it more similar to values measured in cortex. [7]

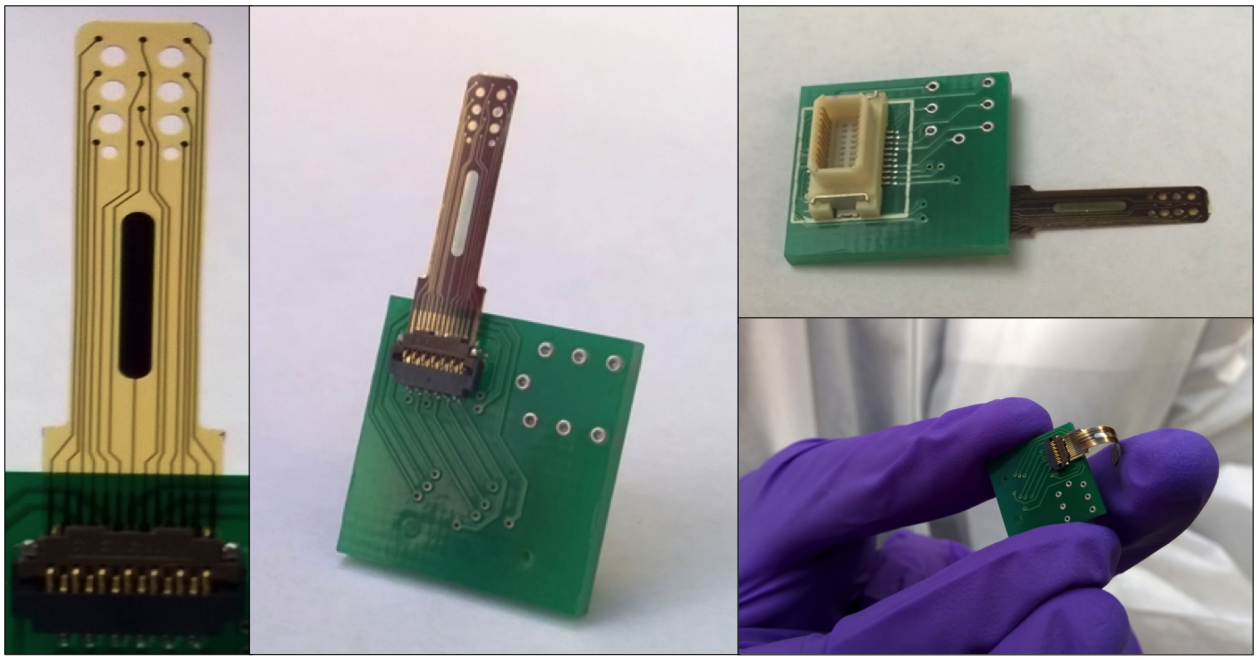

Figure 1.7: μECoG array inserted into a ZIF connector. The PCB routes the ZIF connector to a Hirose 20 pin connector. [7]

about whether any issues with the devices could be attributed to the device design or the GC contacts.

1.4 Purpose

The purpose of this study was to develop a working μECoG array for use with an existing spinal cord injury, rehabilitation study. The Perlmutter Lab is currently using a muscle-activated spinal stimulation protocol to functionally repair damaged spinal cords in a rat model. The lab has plans to implement a motor cortex-activated spinal stimulation protocol because it would allow for the timing between motor cortex sensing and spinal cord stimulation to be adjusted for optimal plasticity effects.

1.4.1 Aim 1

The main goal of this project is to develop a GC μECoG array capable of both sensing and stimulating cortical activity. Stimulus current amplitudes up to 1mA and evoked potential recordings should be attainable. The device needs to cause minimal tissue damage during implant, provide stable recordings over time, and cause a minimal long term tissue response. The device should also be able to interface with existing laboratory hardware.

1.4.2 Aim 2

Based on previous research, I believe there to be a microglial response to chronic stimulation. The second phase of this study would be to use chronically implanted platinum and GC μECoG arrays to look for differences in the long term CI, signal to noise ratios, and histological tissue responses. Within the platinum and GC groups I would have sub groups that either received stimulation or were used for recording purposes only. From this study, I would test the hypothesis that electrical stimulation causes an increased microglia/macrophage response.

Experimental Groups

In order to evaluate the effectiveness of GC μECoG electrodes and investigate the effect of stimulation on tissue response, we designed a study that uses five groups of Long Evans rats. The groups would be composed of 6 rats each and would be as follows: 1) GC electrodes, recording only, 2) GC electrodes, single stimulation channel, 3) GC electrodes, stimulate all channels, 4) Pt electrodes, stimulate all electrodes, 5) Pt electrodes, recording only. Due to the time it took to complete aim 1, aim 2 was not completed and has been left for future consideration.

Chapter 2

METHODS

2.1 Lever Task Training

In order to determine the effectiveness of the carbon and platinum ECoG devices at capturing neural activity related to forelimb movement, I trained Long Evans rats to perform a lever pressing task. When the lever is pressed down a switch is closed (figure 2.1), triggering a time stamp to be recorded by the Neurochip 2.0, a small, programmable computer that sits on the top of the animals arena and contains recording electronics, to record the neural activity and lever time stamps, and stimulating electronics. The time stamps can be used to average the signals recorded from the μECoG array, aligned at the time of lever press.

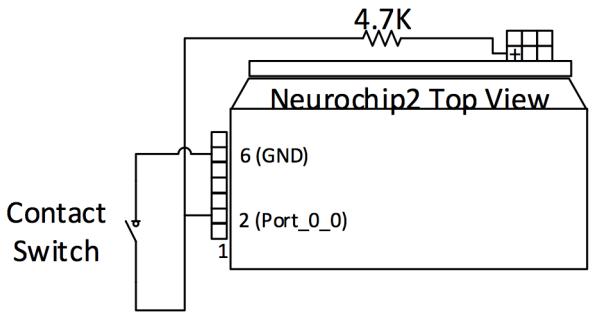

Figure 2.1: Schematic of the lever contact switch connected to the Neurochip 2.0.

Rats are placed in an arena constructed out of clear plastic with two vertical slots (called windows) on the far left and right sides of the front face. The animals are trained to press

the lever in a stable manner (full depression of the lever no more than 4 times successively) at one window and then to retrieve a food reward at the opposite window. There are three basic steps necessary for training. First, rats are introduced to the food reward pellets by leaving a moderate number of them in the animal's home cage. Second, the food reward is associated with the window on the side of the arena opposite the rat's dominant forelimb. This is accomplished by initially placing a small number of reward pellets inside the arena adjacent to the window, and then presenting individual pellets through the window using forceps. Third, the lever press is associated with the food reward. The lever arm is placed in front of the window facing the rat's dominant forelimb (setup in figure 2.1). Using a food reward as bait, the animal is encouraged to reach out of the window with the dominant forelimb. The reward is administered at the opposite window. The behavior is shaped by restricting reward to toward more stable lever presses.

2.2 μECoG Array Implantation in Rat Motor Cortex

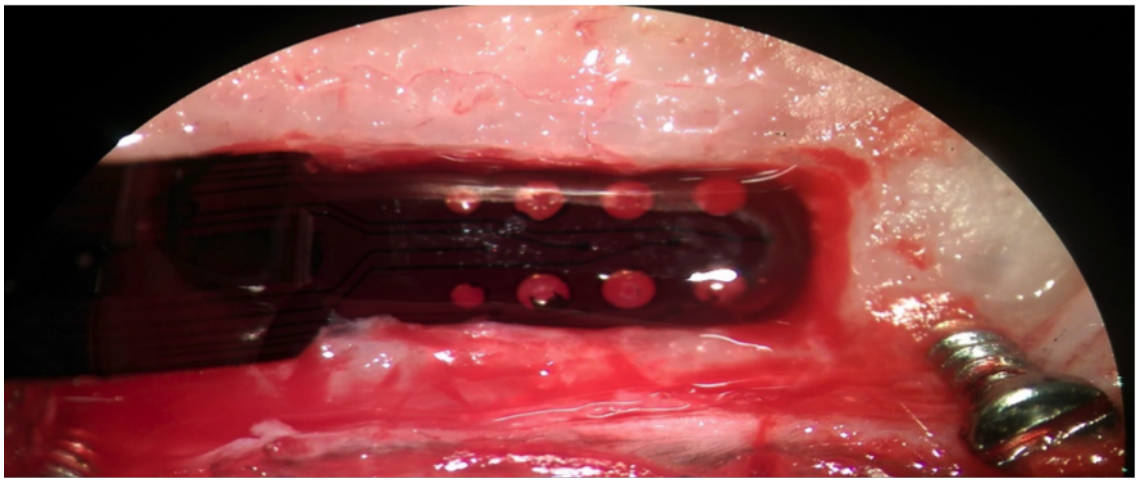

Figure 2.2: Positioning of μECoG array over motor cortex.

1. Prepare animal for surgery

   (a) Give animal Dexamethasone (0.001cc/g) 12 hours before surgery to prevent intracranial swelling.
   (b) Place the animal under anesthesia using isoflurane, shave top of the animal's head, and the secure skull using ear bars in a stereotaxic frame.
   (c) Intraperitoneal injection of: 5cc lactated ringers to prevent dehydration, Dexamethasone (0.001cc/g), Ketoprofen (0.001cc/g) for pain relief, and Baytril (0.2cc) to prevent infection.
   (d) Subdural injection at surgery site: Lidocaine HCl (0.1cc) and Bupivacaine(0.1cc) as local anesthetics.
   (e) Clean incision site by scrubbing with alternating iodine solution and alcohol soaked gauze, 3 times each.

2. Make medial incision, about 2cm long, along the top-center of animal's head. Clear connective tissue.
3. Find Bregma by tapping the skull and looking for the T-shaped suture between the bone plates. Carve the outline of the craniotomy according to figure 2.3 using a curette.
4. Use a drill with a drill bit to make 7-8 screw holes around the craniotomy outline. Insert skull screws in each of the holes, turning no farther than necessary to make secure.
5. Use a drill with a burr bit attached to remove the skull along the boundaries of the outlined craniotomy. Use forceps to remove the skull cap.
6. Use rongeurs to remove the remaining small bits of skull along the craniotomy edge and to create a notch in the lateral-caudal corner (figure 2.3).
7. Wet the dura. Using forceps and micro-scissors, lift the dura and cut a diagonal slice across the craniotomy. Cut away remaining dura within the boundary of the craniotomy.
8. Mix acrylic powder and solution in a small plastic cup and fill a 5cc syringe with the resulting solution. When the solution is thick, coat the caudal skull screws. Make sure

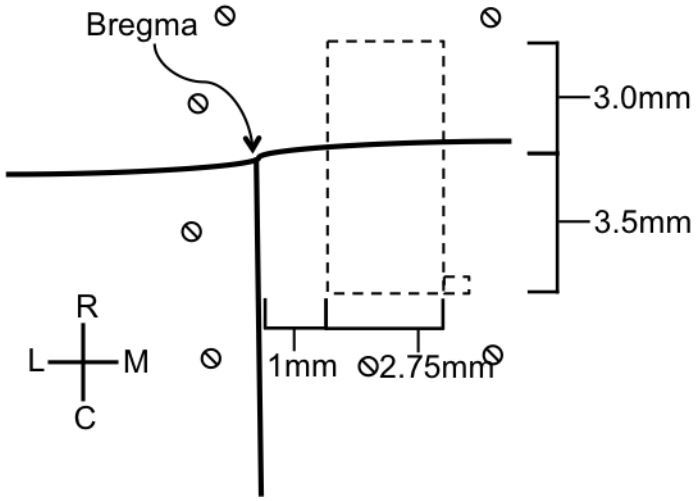

Figure 2.3: Diagram of the craniotomy location and size with skull screw locations shown by a line through a circle. The compass designates surgical directions: rostral, caudal, medial and lateral.

to avoid getting any acrylic in the craniotomy as it will cause tissue damage. Build up the acrylic on top of these screws, about 0.5cm high.

9. Cut ground wires to length and strip insulation back about 2cm.
10. Place μECoG array in craniotomy (figure 2.2) and rest the PCB on the acrylic dam over the caudal screws.
11. Place dampened gel foam over the device, filling the craniotomy on top and behind the device.
12. Wrap ground wires around two skull screws.
13. Apply acrylic around each of the skull screws, over the craniotomy, around the base of the PCB and over any exposed wire or μECoG array. After implant, the animal is likely to scratch at the implant so the connector and the μECoG device must be protected by the acrylic. This also serves to to seal the device around the craniotomy, preventing infection.

2.2.1 Lever Task Recording

The main purpose of this project was to develop an effective μECoG array capable of recording potentials related to forelimb activity in rat motor cortex. To test this capability it was important to record neural activity while the animal performed the lever task.

After an animal has been sufficiently trained and implanted with a μECoG array (see section 2.2), steps were taken to record neural activity. First, the animal was connected to a cable that routed the electrical signals from the μECoG device to the Neurochip 2.0. Then, following the setup of the lever (figure 2.1), the animal was directed to perform 30-50 lever presses per trial, with food rewards between each press.

The Neurochip is programmable for various parameters including sampling frequency, high-pass and low-pass filter bounds, and digital gain. I set the sampling frequency to 2630Hz because it is the only way to record from all three channels at the same frequency. I used a band pass filter between 10-1250Hz because ECoG has better signal to noise ratio when recording from low frequency signals compared to high frequency signals[4]. The digital gain was variable, depending on the strength of each signal. I also set up the time stamps such that only the first contact closure was recorded if there were multiple lever pressings, within a one second window.

2.3 Evoked Potentials (EP)

Evoked potentials provide information about the connectivity between neural populations at different recording sites. During this procedure, stimuli are delivered to one cortical electrode and responses are recorded at other cortical sites. Different current amplitudes are used to determine the lowest amplitude needed to cause a responses at a connected site. An average response to each stimulation amplitude can be generated for each recording site by averaging the signals immediately after each stimulus amplitude. From the average responses we can make inferences about the connectivity between the stimulation and recording sites, determine the minimum stimulation amplitude needed to generate an evoked potential and

generate a full stimulus-response curve.

For this test, I used a USBamp biosignal amplifier (Guger) recording system with a STG4008 stimulus generator (Multichannel Systems). The USBamp was set to sample the signals at 4800Hz with no digital filtering. Each stimulus pulse (of variable amplitude) consisted of a negative leading, biphasic, square waveform. Each phase of the waveform lasted 200μs for a total time of 400μs per stimulus pulse. Stimulus pulses of 0μA, 50μA, 150μA, 250μA, . . ., 850μA were grouped together to form a stimulus train with 332.6ms between the end of one stimulus and the beginning of another. These trains were repeated 50 times with 668ms between each train.

2.4 Complex Impedance

Complex impedance (CI) is a measurement of both the real and imaginary components of impedance. In general, the real component gives information about the resistance of the implanted device and nearby tissue while the imaginary component gives capacitance information about the device-tissue interface and surrounding tissue. These measurements were made using a potentiostat (CHI 700D Electrochemical Workstation). For most CI data collection, the potentiostat was set to measure between 10-10,000Hz with a peak voltage amplitude of 0.1V and no DC offset. 12 data points were collected per decade (factors of 10 on a log scale) using single frequency data collection methods. CI data was gathered for each device in vitro, in a saline solution, to determine if the device was suitable for implantation. After implantation, CI was recorded in vivo multiple times weekly to assess the changes in the device-tissue interface.

2.5 Fabrication of the Glassy Carbon μECoG Arrays

Glassy carbon (GC) μECoG arrays are made using MEMS fabrication processes at San Diego State University (SDSU)[7]. To begin, a silicon wafer is layered with 1-2μm of SiO_2 followed by negative tone SU-8 Photoresist (MicroChem, Boston, MA). A mask is then applied over the SU-8 and the desired GC pattern is achieved through photolithography. Pyrolysis is

then carried out in a closed ceramic tube-furnace (Lindberg Division of Sola Basic Industries of Watertown, WI) with continuous nitrogen flow of at least 2 L/min. The rate of heating and maximum temperature affect the mechanical and electrical properties of the resulting GC (figure 1.5). Polyimide is then spin coated over the construct and lithography is used to expose the GC. This is followed by sputter deposition of chromium (as an adhesion promoter) platinum and gold over the GC and along the array to form the metal traces, ground pad and bump pads. Dimensions are given in figure 2.5. Last, a coat of polyimide is spin coated over the traces to electrically insulate the metal traces and lithography is used to expose the ground pad and bump pads.

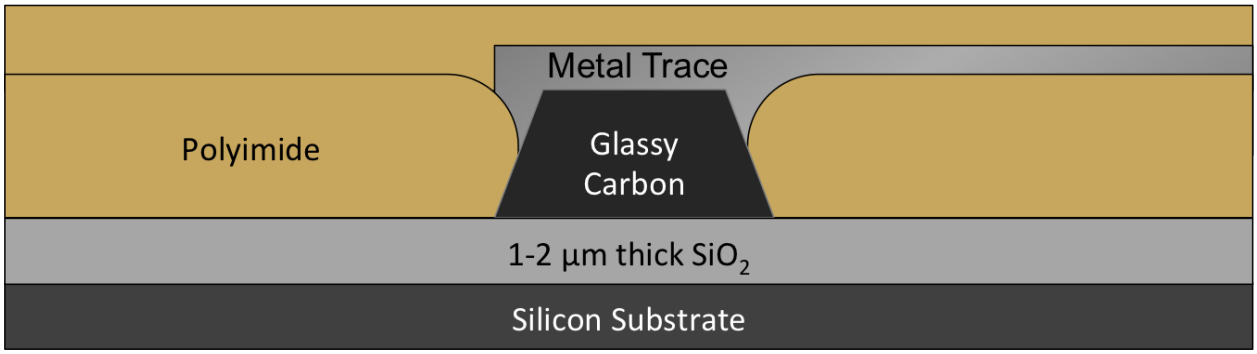

Figure 2.4: Cross section of a GC electrode contact and metallic trace imbedded in polyimide substrate.

It is important that the electrodes be able to record from the same areas in motor cortex for the lifetime of the implant. We therefore incorporated holes throughout the array to facilitate astrocyte encapsulation of the device. We propose that this will serve to anchor the device in place, thereby preventing a shift after implantation. It may also reduce the chronic tissue response because damage can occur if the implant moves relative to the tissue. Furthermore, this acute astrocyte encapsulation may prevent the chronic tissue response from increasing the distance between the neurons and the electrodes over time.

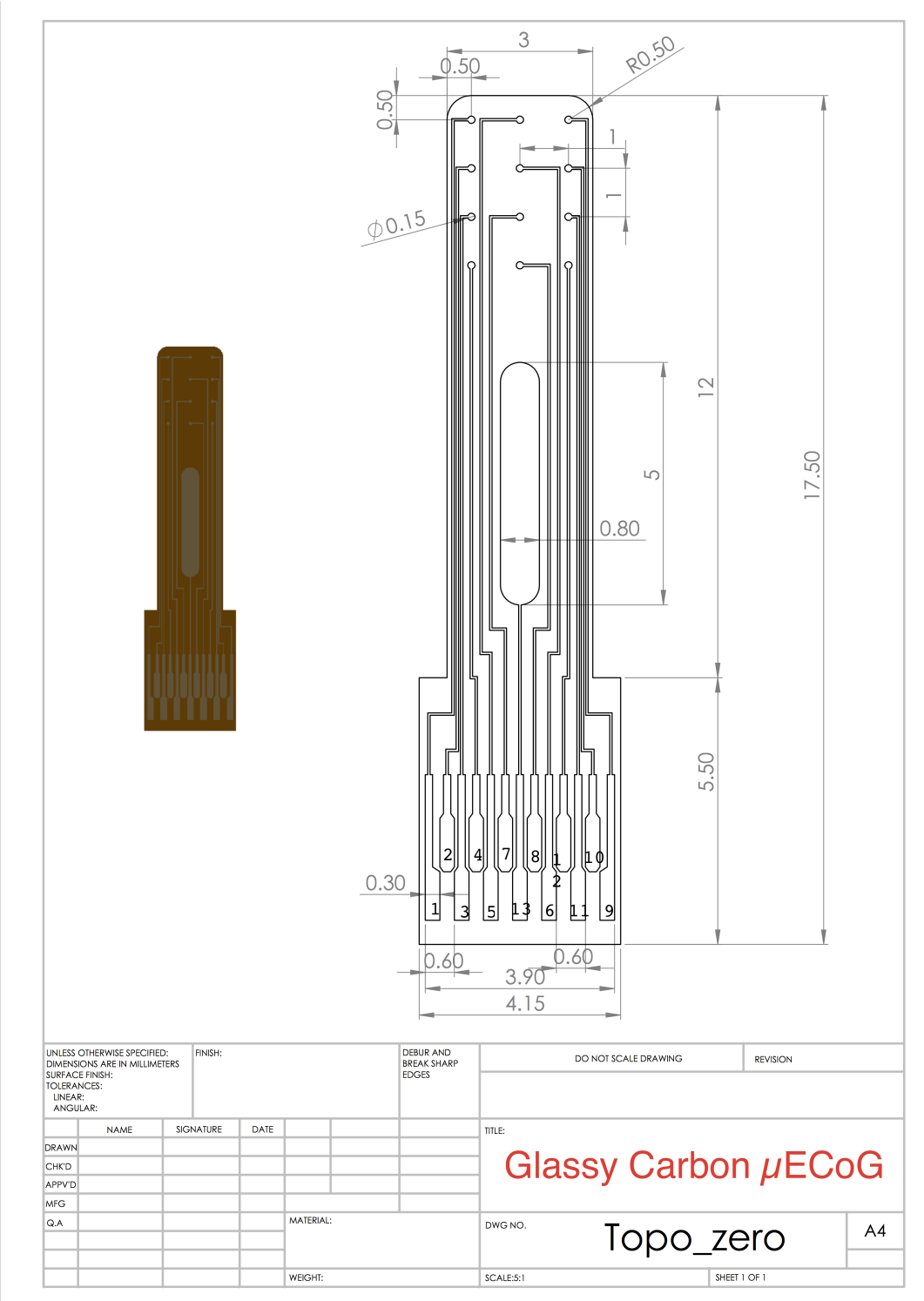

Figure 2.5: Schematic of the μECoG array design. Measurements are given in mm.

2.6 Tissue Histology

Animals were sacrificed for histology by injecting them with a lethal dose of Beuthanasia-D and then perfusing them with paraformaldehyde (4%) after which the brains, with the μECoG devices attached, were removed and placed in paraformaldehyde for 24 hours. Then the brains were placed in HEPES Hanks (HBHS) solution until sliced. Beginning at the caudal end of the device, the brain was sliced into 130μm sections. Each section was stained for astrocytes (GFAP), microglia and macrophages (Iba1), cell nuclei (Hoescht), and neurons, (NeuroTrace). The slices were then imaged using confocal microscopy.

Chapter 3

RESULTS AND DISCUSSION

For our purposes we needed an ECoG array capable of stimulating and recording neural activity while chronically implanted. The device must also be able to interface with our existing hardware.

Many iterations and alterations to the device were made in order to yield a larger fraction of the devices that worked properly. One of the greatest challenges of developing the GC μECoG arrays was that many of the electrode channels presented with high impedance. This is an issue for the reasons listed in section 1.1.1. It is important to note that the high impedance of the electrodes was not due to the GC, but due to the electrical connectivity between the electrode surface and the recording system. In this section, I detail the various issues with our device design and the changes I implemented to increase the yield of usable devices.

3.1 ZIF Opening During Surgery

The zero-insertion force (ZIF) connector (Hirose, FH26), routed through a printed circuit board (PCB), is what allows for electrical connection between a thin film μECoG array and a 20-pin connector (Hirose, DF-17) used by the Perlmutter Lab. Other methods, such as using conductive epoxy to connect directly to the DF-17, have not worked and easily result in damage to the μECoG array. The ZIF connector is specifically designed to secure thin film electronics and is expected to be a reliable way to interface with the arrays.

The first μECoG arrays, which passed tests for functionality at SDSU, were implanted into rat motor cortex upon delivery to the University of Washington (UW). In vivo CI testing showed that the average real impedance for all but animal SDS 05 was around 100MΩ (figure

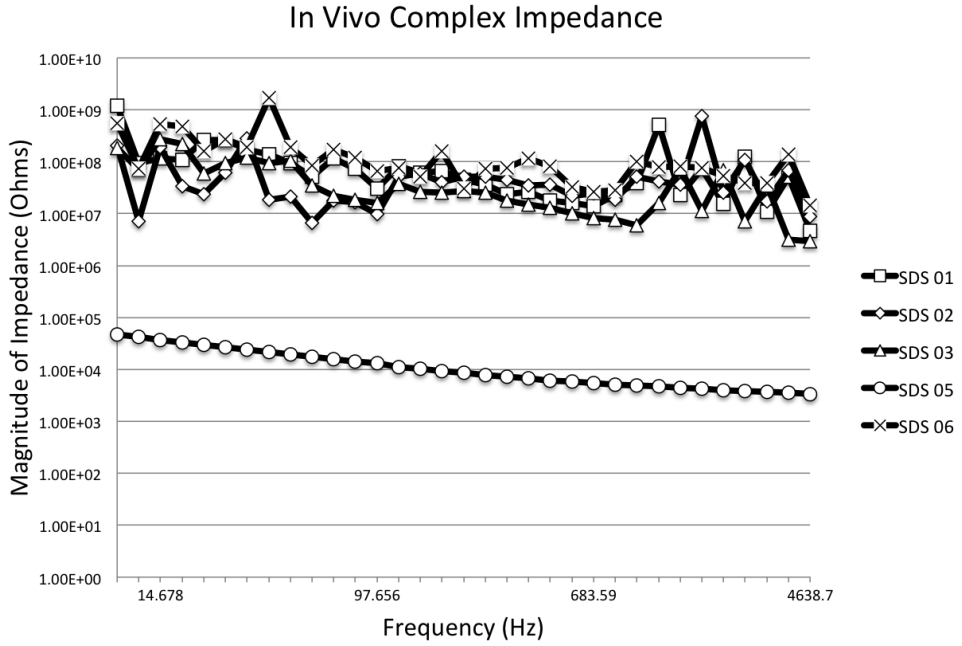

Figure 3.1: Complex impedance from the first batch of implanted animals indicates that the μECoG devices are not electrically connected (animals SDS 01, 02, 03, 04, 06). Animal SDS 05 shows what a connected device's complex impedance should look like.

3.1), indicating that the devices were not electrically connected. This value is close to the upper measurable limit of the potentiostat and is characteristic of a disconnected circuit. Through optical verification of the animals' implants and bench-top recreation I was able to determine that manipulation of the array during surgery caused the ZIF connector to open. This caused electrical contact between the μECoG array and the ZIF to be broken.

One solution to this problem would be to mechanically secure the ZIF connector by applying a coating to maintain closure. For this purpose I investigated the use of epoxy, wax, E6000, and silicone, applied after the connector was attached to the ECoG array. I found that all of these substances prevented the ZIF from opening during surgery, increasing our yield of usable electrodes, however it introduced another problem.

3.1.1 Securing the ZIF Connector

The addition of many coating materials over the ZIF usually caused an increase in the resistance of the electrode circuit. For example, the application of silicone over the ZIF caused a substantial increase in the 1kHz impedance value of all of the electrodes on one array (table 3.1). Impedance values returned to baseline after removal of the silicone, further demonstrating that covering the ZIF with a binding agent can interfere with the electrical contact between the array and the connector. This may be due to fluid seeping into the connector, getting between the bump pads of the array and the pins of the ZIF. If this is the case, the application of acrylic during surgery could also break electrical connectivity.

Electrode A 31												
Contact	1	2	3	4	5	6	7	8	9	10	11	12
Pre Silicone	1.4M	990k	490k	460k	217k	140k	174k	204k	225k	282k	125k	258k
Post Silicone	2.6M	2.5M	1.5M	1.9M	1.3M	1.3M	1.7M	2.0M	1.25M	1.12M	1.1M	2.1M
Remove Silicone	708k	790k	363k	359k	110k	112k	135k	168k	178k	200k	104k	266k

Table 3.1: 1kHz impedance values (Ω) of a GC μECoG array. Measurements were taken before and after the addition of silicone over the ZIF connector. Another measurement was taken after the removal of the silicone.

Parafin wax film (Parafilm) proved to be an acceptable solution to this problem. This method avoided the use of any binding agent while still securing the ZIF flap and preventing acrylic from entering the connector during surgery. The use of Parafilm to secure the ZIF resulted in an increased yield of usable electrodes because fewer good devices were rendered unusable due to covering the ZIF with a binding agent.

3.2 Evoked Potentials (EP)

In order to determine the stimulus current amplitude to use for the stimulation study detailed in Aim 2 (section 1.4.2), I looked at EP data from 4 rats, implanted with electrode arrays whose impedance was below 500kΩ at time of implant, and chose the lowest current amplitude that resulted in an EP at another electrode site. Based on this information I chose a stimulation current of 350μA. However, upon further interrogation we determined that the EP information gathered using the GC devices was actually a stimulation artifact. As an example (figure 3.2), we can see that what should be the largest EP (850μA) is in fact one of the smallest EPs.

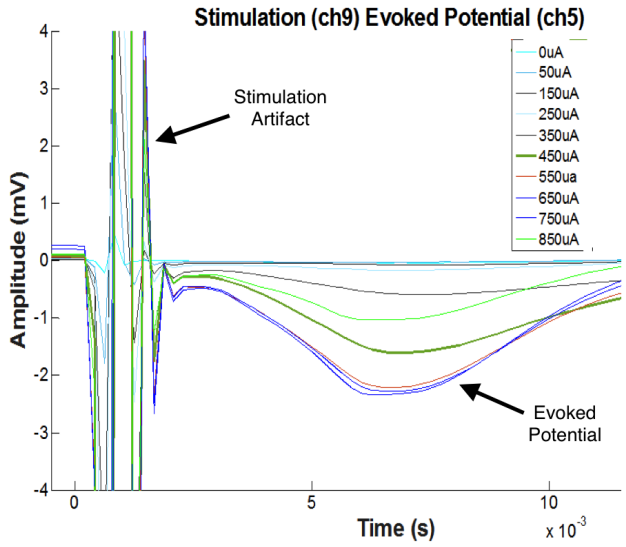

Figure 3.2: Stimulus amplitudes (0, 50, 150, 250, . . ., 850uA) were repeated 50 times at channel 9, recorded at channel 5 and averaged for each amplitude. Each stimulus consisted of a biphasic square wave, 200μs per phase, leading with a negative polarity. The stimulus artifact can be seen immediately after time=0. The signal after this is the evoked potential.

To investigate this anomaly further, I connected two GC implanted animals to a manually controlled stimulator and looked at the windowed average signal in real time. I found that

any current above 150μA resulted in a very strange stimulation artifact. This value also correlated with the stimulator reaching its output limit, where the set amount of current becomes impossible due to the maximum voltage capabilities of the stimulator. The previous evoked potential tests used stimulus trains ramping up to 850μA. The STG4008 does not indicate if the output limit was reached during the trials but this test shows that the amount of current I had programed to be delivered was not possible under the given conditions. Therefore, it was determined that the "EP" responses that I gathered previously were in fact an artifact of the stimulator reaching its output limit and further evidence that the μECoG arrays were not functioning properly.

3.3 Device Thickness

Some μECoG devices had a thickness of 0.1mm while ZIF connector is designed to accept devices that are between 0.2mm and 0.3mm thick. This difference is problematic for a few reasons. Foremost is that the normal forces between the bump pads and the pins inside the ZIF are very small. A stronger mechanical connection would mean a more stable electrical connection. Furthermore, the μECoG device being too thin may make it easier for a binding agent over the ZIF to cause a large impedance increase. Thin devices may allow the liquid epoxy (or other liquid agent) to work its way into the connector and break the connection between the bump pads and the ZIF pins. In order to address these two issues I needed to increase the device thickness.

I proposed that a better mechanical, and therefore electrical, connection between the μECoG array and the ZIF connector could be made by increasing the operational thickness of the array by adding a layer of material to the underside of the bump pads. I performed a survey of available tapes and found that common electrical tape has a thickness of just under 0.2mm. However the mechanical mismatch between the polyimide and the electrical tape proved to be a problem. Within tens of minutes after the electrical tape was applied and the ZIF was closed, the ZIF would open again. The elasticity and mechanical mismatch of the electrical tape, compared to polyimide, probably caused a normal force to be applied

to the flap of the ZIF connector and the device to be deflected upward (figure 3.3). Over time, this force was sufficient to open the ZIF flap.

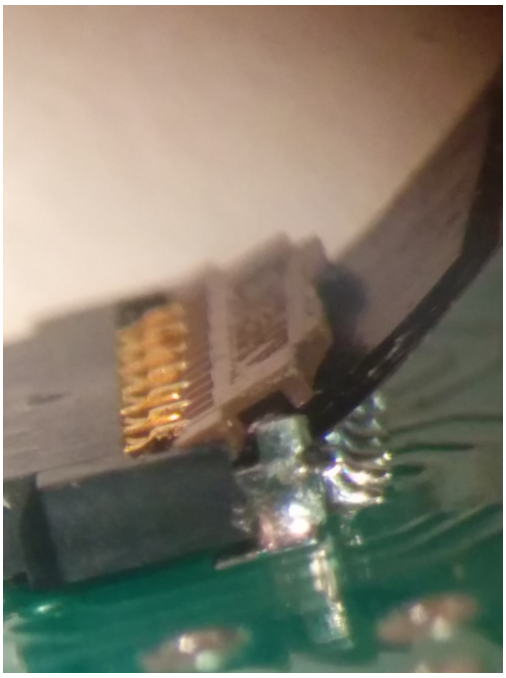

Figure 3.3: Electrical tape added to the back of the polyimide array makes the device thickness within the recommended limits of the ZIF connector but causes the array to be deflected and the ZIF flap to open slowly over time.

Kapton tape is made of polyimide and therefore well-matched to the mechanical properties of the arrays. One minor issue with Kapton tape is that it is significantly thinner than the required 0.1mm, requiring that several layers be applied. As figure 3.4 shows, the application of Kapton tape to reinforce the device thickness did not cause the deflection or latent ZIF opening, as seen with electrical tape. Therefore, the application of Kapton tape to the back of the μECoG device solved the device thickness problem.

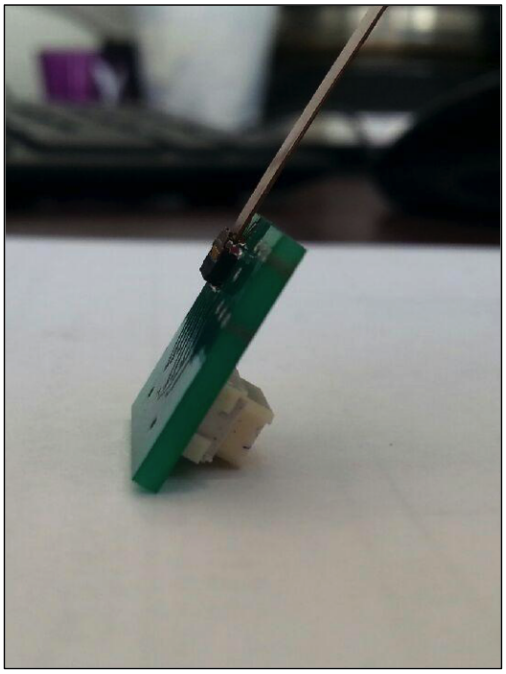

Figure 3.4: Kapton tape applied to the back of the polyimide array makes the device thickness within the recommended upper limit of the ZIF connector without causing device deflection or opening of the ZIF connector.

3.4 Complex Impedance Methods

Some devices that were impedance tested at SDSU and determined to have ideal complex impedance did not pass impedance testing at the UW (figure 3.5). At first, this difference was attributed to the difficulties we were having with the ZIF connector. However, once all ZIF related issues were addressed and the problem continued, I realized that there must be an issue with one of our CI testing techniques.

Using two different impedance meters, I confirmed that there was low resistance in the cable that connected the PCB to the CI testing machine and in the ZIF/PCB interface that connected the cable to the μECoG device. The 1kHz impedance measurements from three different μECoG devices, made with the CH Instruments Electrochemical Workstation, were

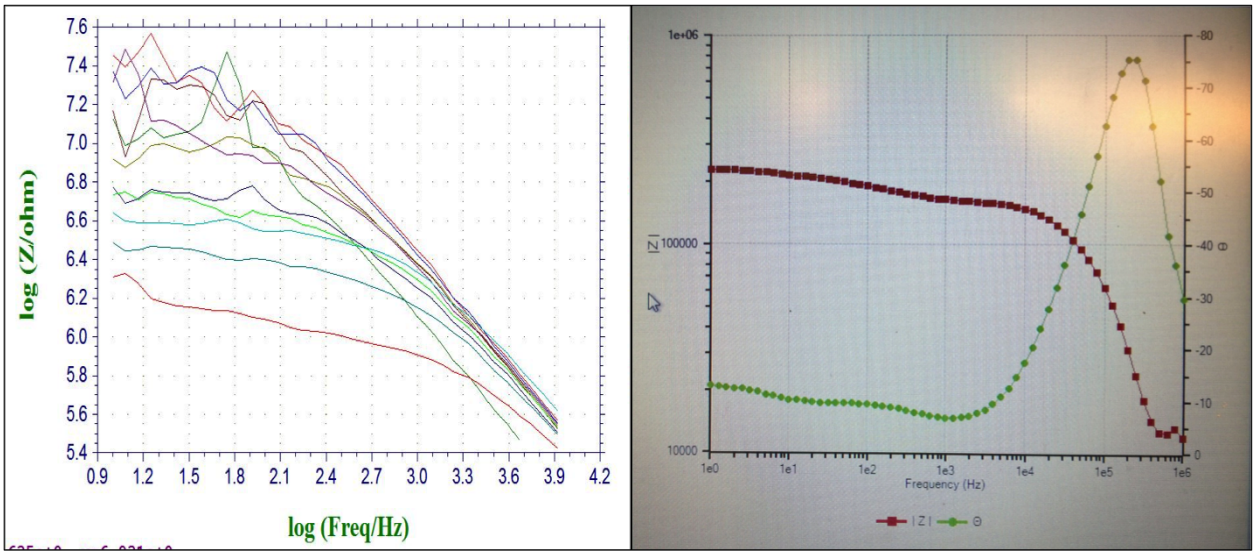

Figure 3.5: Complex impedance graphs collected from the same device. Left is a measurement of all channels recorded at the University of Washington. Right is a measurement of one channel recorded at San Diego State University.

also validated using a separate impedance meter (table 3.2). These results suggested that the CH Instruments Electrochemical Workstation and the parameters under which I used it were a valid means of measuring CI.

Upon further consultation with my collaborators at SDSU, we discovered that the SDSU group measured CI under galvanostatic conditions, while the CH Instruments Electrochemical Workstation used a potentiostatic mode. A galvanostat controls current and measures voltage whereas a potentiostat controls voltage and measures current.

The problem with testing a high impedance electrode with a galvanostat is that the current amplitude cannot be set low enough to prevent the device from reaching the voltage output limit at low frequencies, where the real component of impedance is higher. Note the plateau in the right graph of figure 3.5. When the output limit is reached, the galvanostat measures a voltage that is much lower than what would be required to push the designated

Electrode A11												
Contact	1	2	3	4	5	6	7	8	9	10	11	12
CHI	2.9M	2M	1.9M	330k	1M	900k	1.7M	1.7M	1.4M	1.5M	1.2M	1.7M
BAK	1.8M	1.4M	1.35	325k	1.2M	1.25M	1.7M	1.8M	1.5M	1.5M	1.3M	1.7M
Electrode A16												
Contact	1	2	3	4	5	6	7	8	9	10	11	12
CHI	1.8M	525k	1M	1.7M	620k	603K	1.6M	1.5M	28k	360k	250k	787k
BAK	1.8M	600k	1.35M	1.9M	900k	700k	1.8M	1.75M	35k	360k	300k	900k
Electrode A 31												
CHI	1.4M	990k	490k	460k	217k	140k	174k	204k	225k	282k	125k	258k
BAK	800k	1M	600k	700k	190k	145k	270k	360k	290k	350k	160k	700k

Table 3.2: The $1kHz$ magnitude of impedance (Ω) for several μECoG devices. Two different pieces of equipment (CH Instruments Electrochemical Workstation vs. BAK Electronics Electrode Impedance Meter) were used to validate the measurements.

amount of current. It uses this lower voltage value to calculate the real component of impedance and therefore calculates an artificially low impedance.

A secondary affect of using a galvanostat to measure CI is that the galvanostat will use as much voltage as is necessary, up to the output limit, to push the designated amount of current. This is an issue because the required voltage can be outside the water window, normally -0.6V to +0.8V[1], the voltage beyond which water is split into O_2 and H_2. This extra source of electron carriers allows for more current to pass between the electrode and the ground, creating a parallel pathway to the existing Na^+ and Cl^- charge carriers. This parallel pathway reduces the resistive load between the electrode and ground, contributing to the artificially low impedance.

In comparison, a potentiostat has none of these issues. By controlling the voltage I can be sure that the bounds of the water window are not exceeded and that the voltage is always below the output limit. Furthermore, the resulting current, although very small (around

1nA), is within the measurement capabilities of the potentiostat. It is therefore necessary to use a potentiostat when measuring the CI of μECoG arrays.

3.5 Metal Trace Geometry

After addressing problems involving the ZIF connector and CI testing techniques, it became apparent that there was an issue with the functionality of the μECoG devices. A closer examination of the fabrication process revealed that the GC and polyimide surface that the metal trace was laid upon was not flat, as previous models suggested (figure 3.6). The pyrolysis of SU-8 into GC forms a trapezoidal cylinder due to the fact that atoms are removed during the pyrolysis process, yet the one side is fixed to a SiO_2 wafer, preventing shrinking. The edge of the polyimide around the GC contact is rounded and intersects with the side of the GC, trapezoidal cylinder. This combination of geometries provides a poor surface geometry for the metal trace leading from the electrode contact to the bump pads(figure 3.7). The sharp angle at the intersection of GC and polyimide, combined with the fact that the gold trace is very thin (300nm), causes a stress point where electrical contact can be easily broken or reduced.

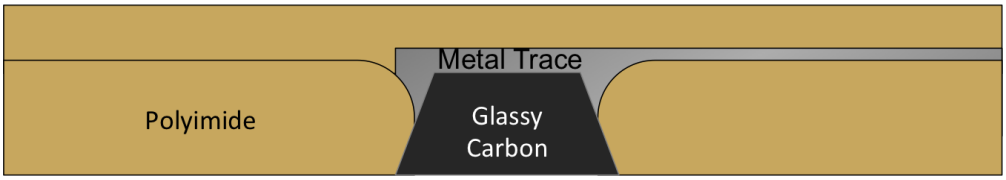

Figure 3.6: Model cross section of a glassy carbon μECoG array depicting what we initially thought the interface between the GC and the metal trace would look like.

I proposed that a decreased diameter hole in the polyamide, such that it was within the top circle of the GC contact, would cause the electrode to be better electrically connected. We also changed the the diameter of the GC contact from 150μm to 300μm, decreased the size of the ground pad from 0.8mm x 5mm to 0.4mm x 2.5mm and decreased the size of

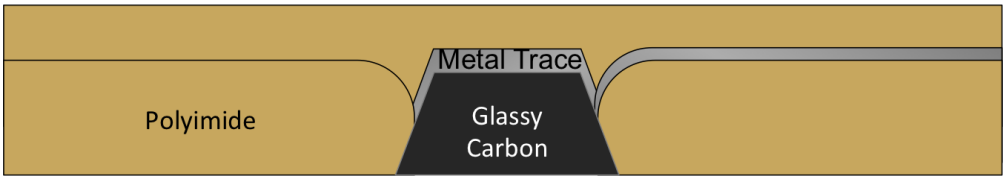

Figure 3.7: Updated model cross section of a glassy carbon μECoG array depicting what the actual interface between the GC and the metal trace would look like.

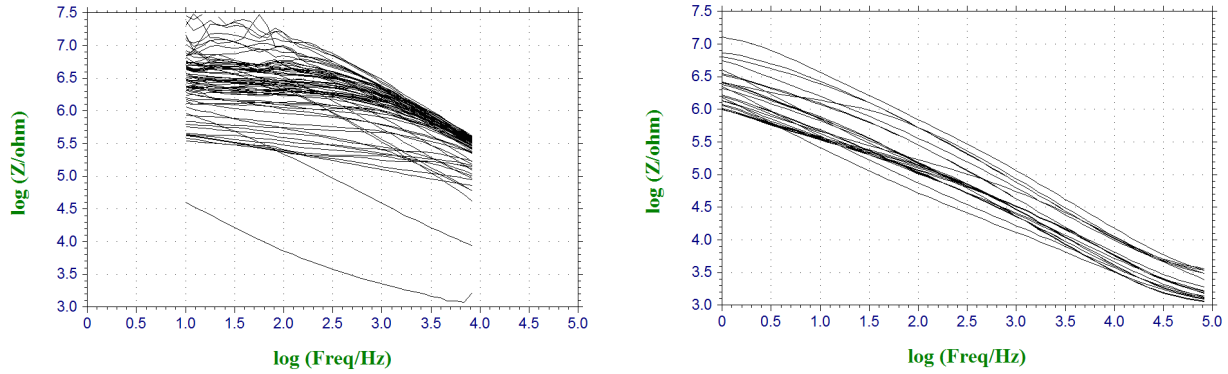

(a) Before

(b) After

Figure 3.8: Magnitude of CI from devices made before and after shrinking the diameter of the polyimide, lithography mask to over the GC electrode contacts

the polyimide lithography holes over the ground and bump pads to be within be bounds of the metal area. In vitro CI tests show that the magnitude of impedance at 1kHz is much lower for devices made using the revised design (figure 3.8), indicating that the electrical connection between the GC contact and the bump pads has been significantly improved.

3.6 Tissue Histology

After 6 weeks of implantation, animals were sacrificed for histology. Initial analysis of the immune response to GC μECoG arrays shows that the GC surface does not cause a significant

immune response. Looking at figure 3.9, we can see that there is virtually no microglial or macrophage (red) response. The astrocyte (green) population is somewhat thicker under the implant. This is most likely due to the removal of the dura during surgery, causing the astrocytes to reform the protective lining.

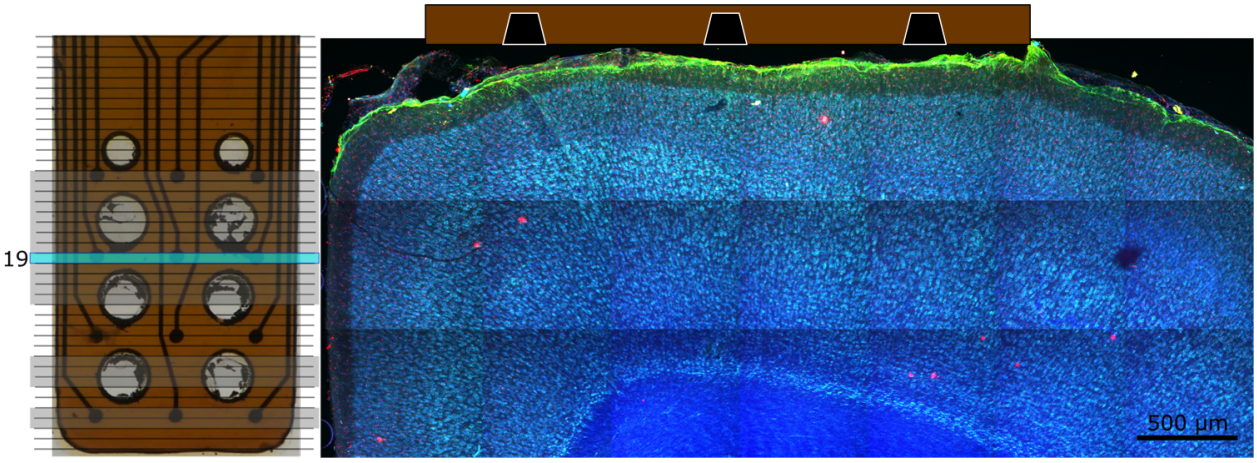

Figure 3.9: Slice of rat motor cortex stained for histological analysis. This slice is a cross section that intersects with three glassy carbon electrode contacts (black). Astrocytes: green (GFAP), Microglia: red (Iba1), Cell Nuclei: blue (Hoescht), Neurons: aqua (NeuroTrace).

Figure 3.10 shows that the astrocytes have grown through the holes that were incorporated into the μECoG device. This is important for long term implants because it allows for better immobilization of the electrode array. This helps provide consistent recording locations and potentially less tissue damage during the lifetime of the implant because the device will not move relative to the brain. It may also reduce the thickness of the astrocyte response after implantation[25], which would help prevent the degradation of signal quality over time.

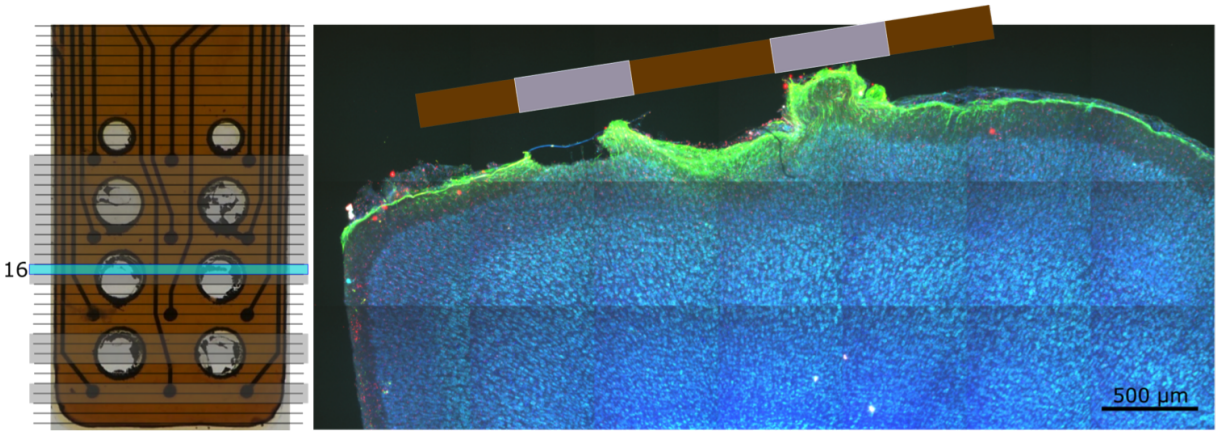

Figure 3.10: Slice of rat motor cortex stained for histological analysis. This area is a cross section that intersects with two through holes (grey) in the polyimide substrate (brown). Astrocytes: green (GFAP), Microglia: red (Iba1), Cell Nuclei: blue (Hoescht), Neurons: aqua (NeuroTrace).

3.7 Summary

Results from this study indicate several things about our GC μECoG array design. Foremost was that our hypothesized function of the through holes was correct. Astrocytes were able to anchor the device in place by growing through these holes. This may also serve to inhibit the astrocyte layer from growing thicker over time due to the device moving relative to the tissue. We also learned that the micro-scale geometry of the device is very important. When using MEMS fabrication techniques, one must take into consideration the geometries of intersecting layers and design them such that the connections are robust. Lastly, we learned that it is possible to create low impedance GC μECoG arrays. In vitro testing shows that GC has been successfully incorporated into a μECoG device and that it is ready for in vivo testing.

3.8 Future Work

The newest iteration of the μECoG arrays are almost ready for the project detailed in aim 2 (section 1.4.2). In order to move forward, in vivo CI needs to be recorded to show that the devices have low impedance after implantation and are able to electrically interface with the neural tissue. After this, EP data needs to be gathered to show that the devices are capable of both recording and stimulating neural activity. Once these criteria have been met, a study to compare the chronic implantation of platinum and GC electrodes should be considered. This study should look for differences in the long term CI, signal to noise ratio, and histological tissue response of the two types of devices.

BIBLIOGRAPHY

[1] X. Beebe and T.L. Rose. Charge injection limits of activated iridium oxide electrodes with 0.2 ms pulses in bicarbonate buffered saline (neurological stimulation application). *Biomedical Engineering, IEEE Transactions on*, 35(6):494–495, June 1988.

[2] R. Biran, D. C. Martin, and P. A. Tresco. Neuronal cell loss accompanies the brain tissue response to chronically implanted silicon microelectrode arrays. *Experimental Neurology*, 195(1):115–126, 2005.

[3] C. S. Bjornsson, S. J. Oh, Y. A. AlKofahi, Y. J. Lim, K. L. Smith, J. N. Turner, and S. J. Kim. Effects of insertion conditions on tissue strain and vascular damage during neuroprosthetic device insertion. *Journal of Neural Engineering*, 3(3):196–207, 2006.

[4] G. Brindley and M. Craggs. The electrical activity in the motor cortex that accompanies voluntary movement. *The Journal of Physiology*, 223(1):28–29, May 1972.

[5] J. P. Harris, A. E. Hess, S. J. Rowan, C. Weder, C. A. Zorman, D. J. Tyler, and J. R. Capadona. In vivo deployment of mechanically adaptive nanocomposites for intracortical microelectrodes. *Journal of Neural Engineering*, 8(4), 2011.

[6] A. C. Ho, M. S. Humayun, J. D. Dorn, L. da Cruz, G. Dagnelie, J. Handa, P.O. Barale, J.A. Sahel, P. E. Stanga, F. Hafezi, A. B. Safran, J. Salzmann, A. Santos, D. Birch, R. Spencer, A. V. Cideciyan, E. de Juan, J. L. Duncan, D. Eliott, A. Fawzi, L. C. Olmos de Koo, G. C. Brown, J. A. Haller, C. D. Regillo, L. V. Del Priore, A. Arditi, D. R. Geruschat, and R. J. Greenberg. Long-term results from an epiretinal prosthesis to restore sight to the blind. *Ophthalmology*, 122(8):1547–1554, 2015.

[7] S. Kassegne, M. Vomero, R. Gavuglio, M. Hirabayashi, E. Özyilmaz, S. Nguyen, J. Rodriguez, E. Özyilmaz, P. V. Niekerk, and A. Khosla. Electrical impedance, electrochemistry, mechanical stiffness, and hardness tunability in glassy carbon {MEMS} ecog electrodes. *Microelectronic Engineering*, 133:36–44, 2015.

[8] T.C. Lin, H.M Chang, C.C. Hsu, K.H. Hung, Y.T. Chen, S. Y. Chen, and S.J. Chen. Retinal prostheses in degenerative retinal diseases. *Journal of the Chinese Medical Association*, 2015.

[9] C. T. Moritz, T. H. Lucas, S. I. Perlmutter, and E. E. Fetz. Forelimb movements and muscle responses evoked by microstimulation of cervical spinal cord in sedated monkeys. *Journal of Neurophysiology*, 97(1):110–120, 2007.

[10] M. Morrell. Brain stimulation for epilepsy: can scheduled or responsive neurostimulation stop seizures? *Current Opinion in Neurology*, 19(2):164–168, 2006.

[11] W. L. Nastuk, M. C. Becker, D. R. Curtis, J. M.R. Delgado, K. Frank, G. Katz, R. D. Keynes, M.J. Kopac, K. S. Lion, R. L. Schoenfeld, A. L. Sorem, E.E. Suckling, G. N. Webb, and M. L. Wolbarsht. *Physical Techniques in Biological Research*, volume V of *Electrophysiological Methods, Part A*. Academic Press, 1964.

[12] M. A. Nicolelis, D. Dimitrov, J. M. Carmena, R. Crist, G. Lehew, J. D. Kralik, and S. P. Wise. Chronic, multisite, multielectrode recordings in macaque monkeys. *Proceedings of the National Academy of Sciences*, 100(19):11041–11046, 2003.

[13] Y. Nishimura, S. I. Perlmutter, and E. E. Fetz. Restoration of upper limb movement via artificial corticospinal and musculospinal connections in a monkey with spinal cord injury. *Frontiers in Neural Circuits*, 7(57), 2013.

[14] I. Osorio, M. G. Frei, S. Sunderam, J. Giftakis, N. C. Bhavaraju, S. F. Schaffner, and S. B. Wilkinson. Automated seizure abatement in humans using electrical stimulation. *Annals of Neurology*, 57(2):258–268, 2005.

[15] C. Peña, K. Bowsher, A. Costello, R. De Luca, S. Doll, K. Li, and T. Stevens. An overview of fda medical device regulation as it relates to deep brain stimulation devices. *IEEE Trans Neural Syst Rehabil Eng*, 15(3):421–424, 2007.

[16] S. M. Perez, A. Shah, A. Asher, and D. J. Lodge. Hippocampal deep brain stimulation reverses physiological and behavioural deficits in a rodent model of schizophrenia. *International Journal of Neuropsychopharmacology*, 16(6):1331–1339, 2013.

[17] V. S. Polikov, M. L. Block, J. M. Fellous, J. S. Hong, and W. M. Reichert. In vitro model of glial scarring around neuroelectrodes chronically implanted in the cns. *Biomaterials*, 27(31), 2006.

[18] A. A. schendel and M. W. Nonte. The effect of micro-ecog substrate footprint on the meningeal tissue response. *Journal of Neural Engineering*, 11, June 2014.

[19] P. Stice, A. Gilletti, A. Panitch, and J. Muthuswamy. Thin microelectrodes reduce gfap expression in the implant site in rodent somatosensory cortex. *Journal of Neural Engineering*, 4(2):42–53, 2007.

[20] H. G. Tan, K. H. Kong, C.Y. Shee, C.C. Wang, C.T. Guan, and W.T. Ang. Post-acute stroke patients use brain-computer interface to activate electrical stimulation. *Engineering in Medicine and Biology Society (EMBC), 2010 Annual International Conference of the IEEE*, pages 4234–4237, August 2010.

[21] J. N. Turner, W. Shain, D. H. Szarowski, M. Andersen, S. Martins, M. Isaacson, and H. Craighead. Cerebral astrocyte response to micromachined silicon implants. *Experimental Neurology*, 156(1):33–49, 1999.

[22] R. J. Vetter, J. C. Williams, J. F. Hetke, E. A. Nunamaker, and D. R. Kipke. Chronic neural recording using siliconsubstrate microelectrode arrays implanted in cerebral cortex. *IEEE Transactions on Biomedical Engineering*, 51(6):896–904, 2004.

[23] M. P. Ward, P. Rajdev, C. Ellison, and P. P. Irazoqui. Toward a comparison of microelectrodes for acute and chronic recordings. *Brain Research*, pages 183–200, 2009.

[24] J. C. Williams, J. A. Hippensteel, J. Dilgen, W. Shain, and D. R. Kipke. Complex impedance spectroscopy for monitoring tissue responses to inserted neural implants. *Journal of Neural Engineering*, 4(4):410–423, 2007.

[25] B. D. Winslow, M. B. Christensen, W. Yang, F. Solzbacher, and P. A. Tresco. A comparison of the tissue response to chronically implanted paryleneccoated and uncoated planar silicon microelectrode arrays in rat cortex. *Biomaterials*, 31(35):9163–172, 2010.